1-1-2015

Development of a novel variable stiffness and damping magnetorheological fluid damper

Shuaishuai Sun
University of Wollongong, ss886@uowmail.edu.au

Jian Yang
University of Wollongong, jy937@uowmail.edu.au

Weihua Li
University of Wollongong, weihuali@uow.edu.au

Huaxia Deng
Hefei University of Technology

Haiping Du
University of Wollongong, hdu@uow.edu.au

See next page for additional authors

Development of a novel variable stiffness and damping magnetorheological fluid damper

Abstract

This paper reports a novel magnetorheological fluid (MRF)-based damper, which synergizes the attributes of variable stiffness and damping through the compact assembly of two MRF damping units and a spring. The magnetic field densities of the two damping units were analyzed. After the prototype of the new MRF damper, a hydraulically actuated MTS machine was used to test the damper's performance, including stiffness variability and damping variability, amplitudedependent responses and frequency-dependent responses. A new mathematical model was developed to describe the variable stiffness and damping MRF damper. The successful development, experimental testing and modeling of this innovative variable stiffness and damping MRF damper make the true design and implementation of the concept of variable stiffness and damping feasible.

Keywords

magnetorheological, development, novel, variable, damper, stiffness, damping, fluid

Disciplines

Engineering | Science and Technology Studies

Publication Details

Sun, S., Yang, J., Li, W., Deng, H., Du, H. & Alici, G. (2015). Development of a novel variable stiffness and damping magnetorheological fluid damper. Smart Materials and Structures, 24 (8), 085021-1-085021-10.

Authors

Shuaishuai Sun, Jian Yang, Weihua Li, Huaxia Deng, Haiping Du, and Gursel Alici

Development of a novel variable stiffness and damping magnetorheological fluid damper

Shuaishuai Sun[1], Jian Yang[1], Weihua Li*[1], Huaxia Deng*[2], Haiping Du[3], and Gursel Alici[1]

[1]School of Mechanical, Materials and Mechatronic Engineering, University of Wollongong, Wollongong, NSW 2522, Australia

[2]School of Instrument Science and Optoelectronics Engineering, Hefei University of Technology, Hefei, Anhui, 230027, China

[3] School of Electrical, Computer & Telecommunications Engineering, University of Wollongong, Wollongong, NSW 2522, Australia

Corresponding Authors: weihuali@uow.edu.au and hxdeng@hfut.edu.cn

Abstract

This paper reports a novel magnetorheological fluid (MRF)-based damper, which synergizes the attributes of variable stiffness and damping through the compact assemble of two MRF damping units and a spring. The magnetic field densities of the two damping units were analyzed. After the prototype of the new MRF damper, a hydraulically actuated MTS machine was used to test this damper performance, including stiffness variability and damping variability, amplitude-dependent responses, and frequency-dependent responses. A new mathematical model was developed to describe the variable stiffness and damping MRF damper. The successful development, experimental testing, and modelling of this innovative variable stiffness and damping MRF damper make the true design and implementation of the concept of variable stiffness and damping become feasible.

Keywords: Magnetorheological fluids, variable stiffness and damping, damper performance, vibration control.

1. Introduction

Speaking of the solutions to addressing the undesired vibrations, stiffness and damping are fundamental yet important mechanical features to be controlled for many technical systems to achieve a desired dynamic behavior. Vibration reduction has been inevitably connected to the concepts of variable damping and variable stiffness, wherein ‘variable’ means controllability, real-time, and reversibility. The variation of damping will induce a change on the resonance magnitude through adjusting the dissipated vibration energy, and the variable stiffness will change the vibration transmissibility by changing the natural frequencies of the controlled system. In view of the powerful potential on the vibration reduction, extensive research or studies have been conducted or carried on with the concept of variable stiffness or damping [1-4].

The controllability of stiffness or damping belongs to one of the most heated vibration control methods, semi-active control, which fills the gap between the active control and the passive control by synergizing the advantages yet getting over the disadvantages of both active and passive control systems. One of the clear advantages of semi-active control over the passive control is that semi-active control can act real time control while maintaining the fail-safe function. In addition to offering comparable control effect, when compared to the active control, semi-active control also provides an energy efficient solution to reducing vibrations. To this end, controlling the damping or stiffness in a semi-active way has been an attractive research solution. And a popular and feasible way of implementing the variable stiffness or damping, currently, is based on the magnetorheological and electrorheological materials based devices [5, 6]. Magnetorheological fluid (MRF) dampers are typical semi-active dampers with variable damping capability and have been widely used for vibration attenuation due to their reliability and fast response [7-9]. Yu’s group has mounted four MR dampers to a full car and tested the system on different types of roads [10]. Yao et al. employed a skyhook control strategy to control an MR damper for a vehicle suspension system [11]. Their experimental results confirmed that the MRF damper is effective on reducing the vibrations induced by the road irregularity [12, 13]. Variable stiffness device is another development for vibration reduction. Youn and Hac developed a variable stiffness

suspension by employing semi-active air spring to vary the suspension stiffness among three discrete values [14]. The experimental result verified the effectiveness of variable stiffness on vibration control. However, compared with MR technology, variable stiffness air spring is complicated and costly because the air pressure must be controlled by an air pump. A typical device for vibration reduction based on magneto-rheological technology is magneto-rheological elastomer (MRE) isolator which is usually used but not limited to protect structures from earthquake [15, 16]. For instance, Li et al. fabricated a new and highly adjustable MRE isolator which increased the force by up to 1579% and the stiffness by up to 1730%.

Based on the successful implementation of variable stiffness or damping devices, new research directions have been originated because of the appearance of dual controllability of stiffness and damping [17-19]. The effectiveness of variable stiffness and damping on vibration reduction has been fully verified through simulation [20-22], however, a practical device that stiffness and damping are controllably simultaneously has been seldom developed. The work reported by Spelta et al. [20] and Xu et al. [21] are the conceptual designs of variable stiffness and damping structure. Their simulation applied the variable stiffness and damping device on a vehicle suspension and the results verified that it is better at reducing vibrations than the suspension with only variable damping. Greiner-Petter et al. [23] presented a semi-active MRF mechanism which offers a variable stiffness and damping by utilizing two magnetorheological fluid valves and two springs. The experimental results indicate that the damping of this system can vary continuously but its effective stiffness has only three limited values. Zhang et al. [24, 25] developed a variable stiffness and damping MR valve based isolator, whose dynamic response showed that the stiffness of the isolator can be adjusted in a relative large range. However, the structure is complicated and not compact which make it hard to find real applications. To overcome these disadvantages, this paper is oriented to report an innovative MRF damper whose stiffness and damping can be controlled. Also, the structure of the new MRF damper is compact, which make it suitable for practical usage. The core design of this MRF damper is ingenious combination of two MRF cylinders and a spring. Its most valuable features include its compactness, dual and individual controllability of

stiffness and damping. The paper is organized by the following manners. Section 2 gives a detailed introduction about the design and the working principle. Section 3 analyses the feasibility of its magnetic field design and the experimental setup is shown in Section 4. Section 5 includes the analysis and discussion of the experimental results and a model is explained for the MRF damper in Section 6. Section 7 draws the conclusion.

2. Design of the innovative MRF damper

2.1. The structure of the MRF damper

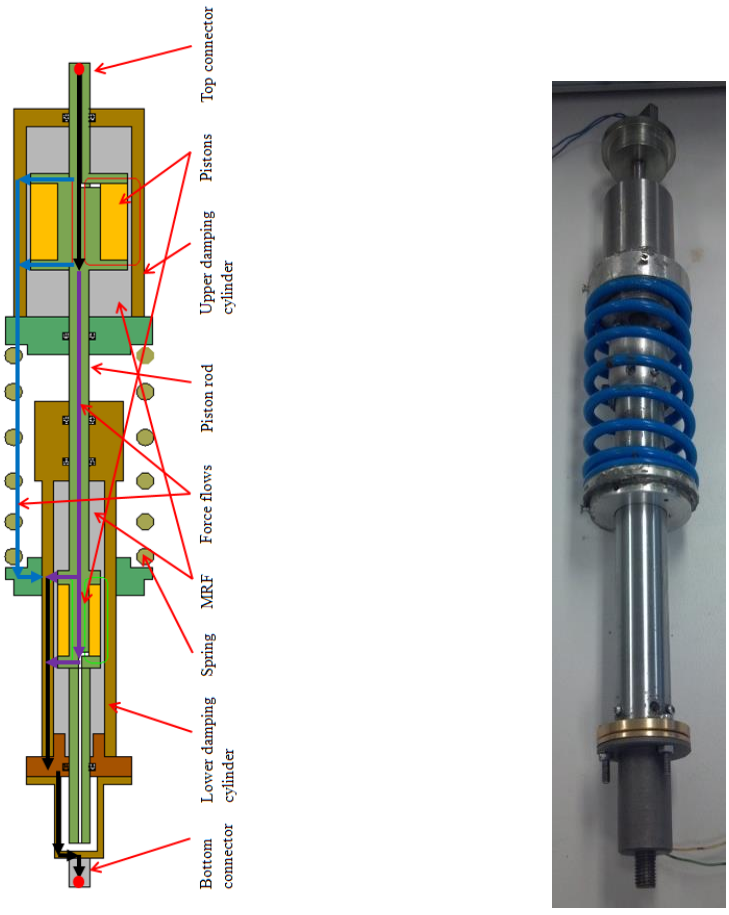

(a) Schematic (b) Prototype

Fig.1. Design drawing and prototype of the MRF damper: (a) schematic; and (b) prototype.

Fig.1 shows the design drawing of the innovative MRF damper which is mainly composed of a spring, a piston rod, two pistons with two sets of electromagnetic coils, some seals, and connectors. The piston rod runs through two damping cylinders, namely the upper damping cylinder and the lower damping cylinder, each damping cylinder possessing a set of

electromagnetic coil energizing the magnetorheological fluids (MRFs) filled in the reserves. The piston rod also can have relative movement with the two cylinders. The spring acts as the connection between the two damping cylinders and provides stiffness when these two cylinders have relative motions. The electromagnetic coils extend coaxially around the support structure, e.g. the piston, such that direct currents, I_1 and I_2, passing through the coil generates magnetic fields. The upper damping force and the lower damping force are controllable by the regulation of I_2 and I_1, respectively.

The most innovative design of this MRF damper is the synergy of variable stiffness and variable damping through the compact assemble of two damping cylinders and a spring. It is achieved by controlling the rheological properties of MRF filled in the two damping cylinders. In particular, the stiffness and the damping can be controlled individually and the stiffness can change from the minimum stiffness of near 0 N/m.

2.2 Working principle

The achievement of stiffness variability and damping variability is based on the rheological characteristics of MRF that its damping will increase as the applied magnetic field strengthens. The variable damping characteristic is mainly dependent on the outputs of the lower damping cylinder. When the applied current I_1 is small, the damping and damping force from the lower damping cylinder is relative small, however, tend to be bigger as I_1 grows. The variable stiffness property is determined by the upper damping cylinder together with the spring whose lower connection of the spring is fixed with the lower damping cylinder. The upper damping cylinder works in series with spring, which makes it possible to control the effective stiffness of the new MRF damper by controlling the damping of the upper damping cylinder. In order to illuminate the working mechanism of the proposed damper in a clear way, force analysis is included. As shown in Fig.1(a), there are two ways of force flow: (i) one way is that force passes from the rod of the upper damper to the piston, then to upper cylinder and finally to the cylinder of lower damper through the spring (blue line in Fig. 1(a)); (ii) the other way is the force passes through the rod of the upper damper to the piston of the lower damper, then to the cylinder of the lower damper (the purple line in Fig.1(a)). These two force flows can be controlled independently by changing the currents of the coils. The stiffness variation of the

damper is mainly controlled by the blue force flow while the damping is mainly controlled by the purple one. In terms of the stiffness variation, if I_2 is zero or sufficiently small the damping force in the upper unit is small, which results in relative motion between the piston rod and the upper damping cylinder when the piston rod moves into the damper. In such case, as the deformation of the spring is small, it contributes very little stiffness to the damper. Therefore, the effective stiffness of the damper is small. On the other hand, when I_2 increases gradually, an increasing upper damping force will be generated. It will, therefore, become more difficult for the piston rod to move through the upper damping cylinder. In this case, the upper damping cylinder moves together with the piston rod, which leads to the deformation of the spring and consequently varies the effective stiffness of the damper. Thus the bigger the I_2 is, the bigger the effective stiffness is. In addition, the damping of the lower damping cylinder is controlled by I_1. The bigger the I_1 is, the bigger the overall damping.

3. Magnetic field analysis of the new MRF damper

3.1 Analysis of the magnetic field density

The magnetic fields generated by coils are important to induce changes to the viscosity of the MRF fluid. In this subsection, the magnetic fields around pistons are carefully calculated and analyzed. Fig. 2 illustrates the magnetic circuit for both of the two pistons because their structures are the same. The detailed parameters for both of the two damping units are shown in table 1. The magnetic resistances of each segment are calculated by the following equations.

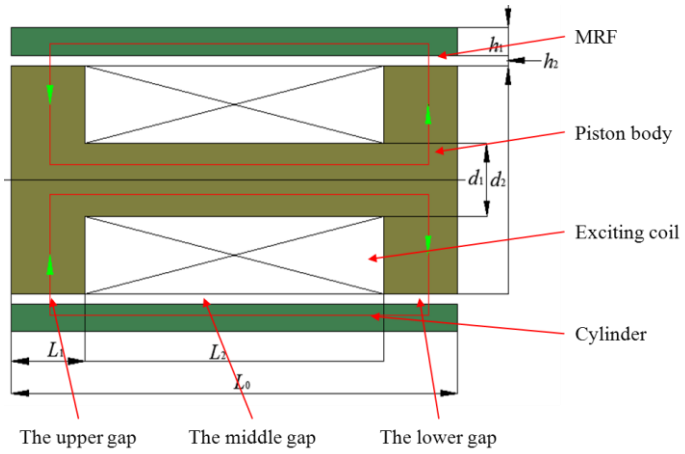

Fig. 2. The sketch of the damping unit

Table 1. Parameters for both damping units

(a) Upper damping unit

Parameters	Value		Parameters	Value
h_1	4mm		L_1	6mm
h_2	1mm		L_2	35mm
d_1	15mm		L_O	47mm
d_2	30mm		Turns of coil	800

(b) Lower damping unit

Parameters	Value		Parameters	Value
h_1	3mm		L_1	6mm
h_2	1mm		L_2	40mm
d_1	10mm		L_O	52mm
d_2	22mm		Turns of coil	500

The magnetic resistance of the central axis of the two pistons can be calculated by:

$$R_1 = \frac{L_1+L_2}{\pi(d_1/2)^2\mu_1} \quad (1)$$

The magnetic resistance of the flank is:

$$R_2 = \frac{d_2/2}{\pi(d_2/2)L_1\mu_1} \quad (2)$$

The magnetic resistance of the gap is given by:

$$R_3 = \frac{h_2}{\pi(d_2+h_2)L_1\mu_2} \quad (3)$$

The magnetic resistance of damper cylinder is defined as

$$R_4 = \frac{L_1+L_2}{\pi[(d_2/2+h_1+h_2)^2-(d_2/2+h_2)^2]\mu_1} \quad (4)$$

where the μ_0 is the vacuum permeability and μ_1 is the permeability of the 10# steel, μ_2 is the permeability of MRF.

The overall magnetic resistance is given by

$$R_m = R_1+2R_2 + 2R_3+R_4 \quad (5)$$

Thus the magnetomotive force can be calculated based on Ohm's law:

$$\mathrm{NI} = B_0S_0R_m \quad (6)$$

Where B_0 is the magnetic flux density of resistance gap and S_0 is the flux area of resistance gap.

3.2 Simulation analysis using the FEM method

As shown in Fig. 2, the MR damper analyzed in this section composes of the piston body, the cylinder, the exciting coil, and the resistance gap. The piston body and the cylinder were made of No. 10 steel and its permeability is defined by the B-H curve of No. 10 steel shown in Fig.3 (a). The exciting coil is made of copper wire whose relative permeability is 1. The resistance gap is filled with MR fluid (MRF-132DG) from LORD Company. Its permeability is obtained by the B-H curve of MRF-132DG which is shown in Fig.3 (b). 800 and 500 turns of copper wires with diameter of 0.5 mm are used to build the upper piston coil and lower piston coil, respectively. The current density in the exciting coil in this simulation was set at 2.5 A/mm^{-2}.

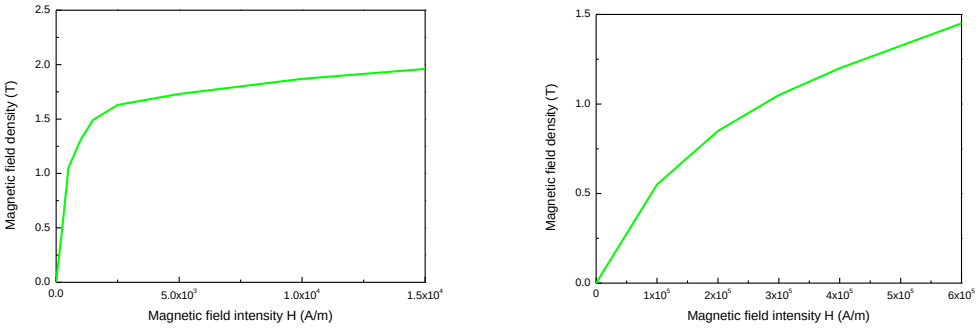

(a) 10# steels (b) MRF-132DG

Fig.3. The B-H curve of 10# steels and MRF

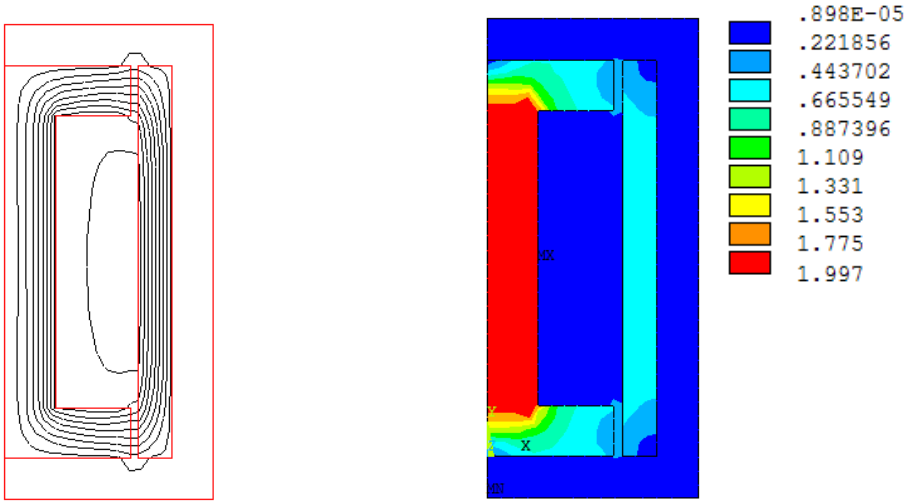

(a) Distribution of the magnetic flux line (b) Magnetic field density

Fig.4. The simulation results of the upper damping unit

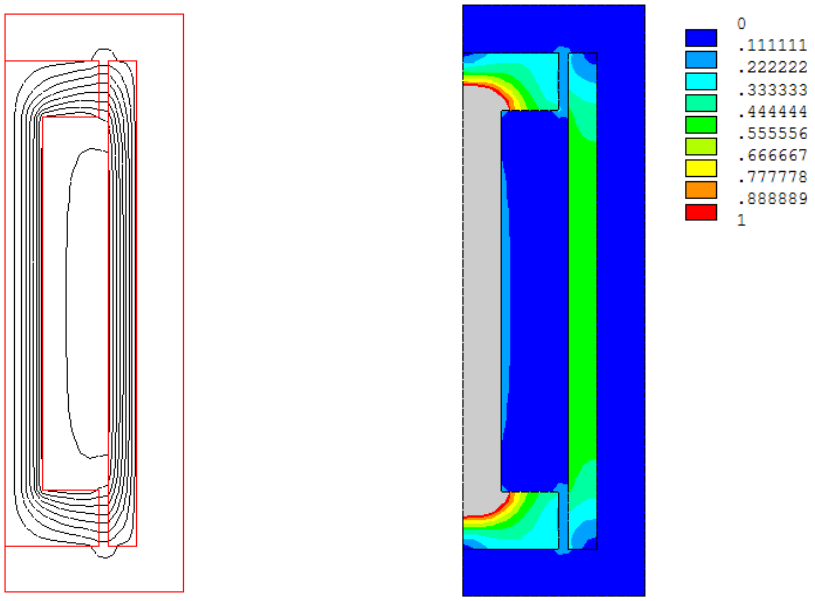

(a) Distribution of the magnetic flux lines (b) Magnetic field density

Fig.5. The simulation results of the lower damping unit

The simulation result of the upper damping unit with 1A current is shown in Fig. 4. Fig.4 (a) shows distribution of the magnetic flux lines. The lines illustrate that piston body, cylinder and the gaps between them enclose the magnetic circuit. Fig. 4(b) demonstrates the magnetic field density of the upper damping unit. This figure illustrates the magnetic field in the upper gap and the lower gap reaches 302 mT. The simulation result of the lower damping unit is shown in Fig.5. In order to clearly show the magnetic field in the gap area, the display range of magnetic field flux density in Fig.5 is set from 0T to 1T. The area with above 1T magnetic field flux density is shown in gray. The simulation result is similar to the upper damping unit except that its magnetic field flux density in the gap is 196mT when the current was set at 2A.

4. Test of the Dynamic Performance

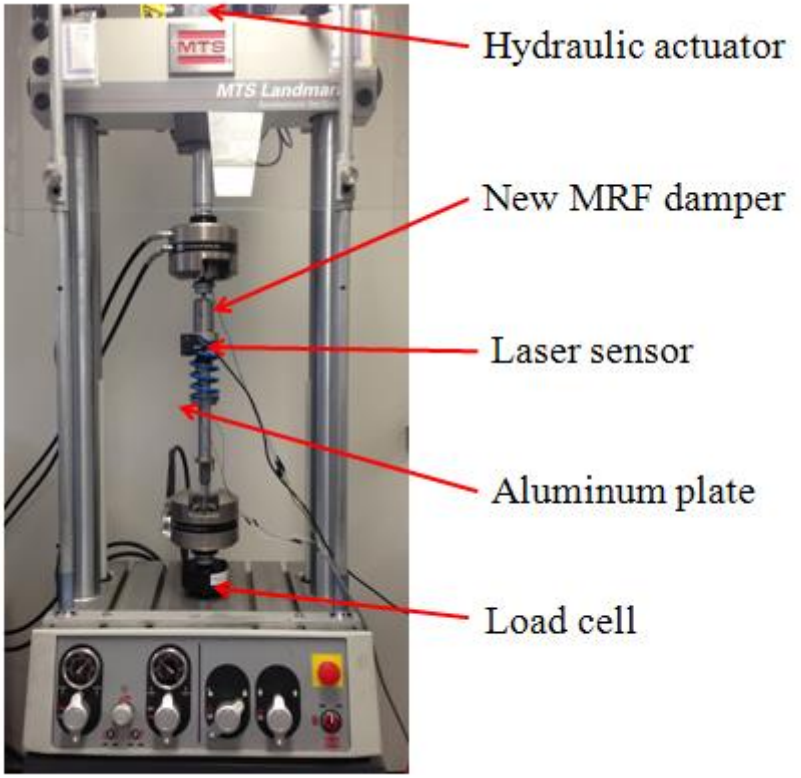

Fig.6. Experimental set up.

As shown in Fig.6, the proposed variable stiffness and damping MRF damper was clamped by a computer-controlled MTS machine (Load Frame Model: 370.02, MTS Systems Corporation), between two coaxially mounted Linear-variable Displacement Transducer (LVDT Part Number 39-075-102, MTS Systems Corporation). The MTS machine was driven by a servo hydraulic system capable of exerting large axial loads onto the test specimen. The damper test system provides harmonic excitation to the damper and records signals taken through the load cells. The signals were saved to a computer via a data acquisition (DAQ) board measuring various feedback data series, namely time, axial displacement, and axial force. During the experiments, a DC power supply was used to generate current to the coils. Once the damper was mounted on the MTS machine through two ends connectors, a predefined sinusoidal routine was programmed into the control software in order to maintain consistency in the testing.

The experiment part has included testing cases for stiffness variability, damping variability, frequency-dependent response, and amplitude-dependent response. Sufficient cycles have

been measured for each single testing case to ensure the performance stability and uniformity. The excitation signal chosen for the field-dependent testing was a sinusoidal wave with a single frequency of 0.1 Hz and amplitude of 10 mm. To obtain the field-dependent response in terms of the variable stiffness, the current (I_2) applied to the upper damping cylinder was varied from 0A to 1A with a step of 0.5A while the current (I_1) applied to the lower damping cylinder was set as 0A. As for the field-dependent response of variable damping, the current, I_1, was set as 0A, 1A, and 2A, respectively, with I_1 maintained as a constant of 0A. In addition to the field-dependent responses, the effectiveness of changing the loading frequency and amplitude on the device performances was also investigated. The loading frequency of the predefined sinusoidal routine was changed to 0.1 Hz, 0.5 Hz, and 1 Hz, respectively, to obtain the frequency-dependent performances; and the amplitude was changed among 5 mm, 7.5 mm, and 10 mm, respectively, for the amplitude-dependent responses. For these two testing cases, both the upper current and the lower current were set as 0A. In order to measure the spring deformation under different I_2, a laser sensor (KEYENCE LB01) was mounted on the top of the spring and an aluminum plate is mounted on the bottom of the spring.

5. RESULTS AND DISCUSSION

5.1 Stiffness Variability

Fig. 7 shows a series of stable force-displacement loops under the condition of I_1=0A and I_2=0A, 0.5A, and 1A, respectively. The experimental results in Fig. 7 clearly show that the output force is a piecewise function of the input displacement in a clockwise direction. In order to give a clear explanation of how the force-displacement loop progresses, the response under the condition of I_2=0.5A and I_1=0A was taken as an example. It is seen that letters are placed clockwisely as indicators of each inflection. In segment AB, a mutation force is generated because the applied external force need to overcome the rod bearing friction and initial damping force from the lower MRF damper so as to allow the relative motion between the piston rod and the lower damping cylinder even though their relative displacement is very small at this stage. When the external force increases gradually to overcome the lower damping force and its rod bearing friction, the piston rod starts to move into the lower

damping cylinder. As the current applied to the lower damper increases, the initial damping force of lower damping cylinder increases, which results in the increase of the segment AB length. The current (I_2) applied to the upper damper, however, determines whether there is a relative motion between the piston rod and the upper damping cylinder. When the current (I_2) is very big, the upper damping force is accordingly big, the upper damping cylinder will move down together with the piston rod. As a result, the spring will be compressed and the stiffness of this variable stiffness and damping MRF damper can be represented by the stiffness of the spring at this stage, which is shown by Segment BC in Fig.7. As the spring is increasingly compressed, the resultant elastic force is increasing. When the elastic force increases to be equal to the damping force of upper cylinder, the upper damper and the spring will remain approximately motionless even though the piston rod keeps moving down. The stiffness of this stage can be regarded as zero, and that's why segment CD is approximately parallel to X-axis. The effective stiffness of this MRF damper is the slope of the line AD which can be calculated by equation (7). And this slope will change as the value of the current (I_2) changes.

This process is reversed when the piston rod moves out of the damper. As observed from Fig.7, the inverse process is symmetrical to the regular process because segments AB, BC and CD are approximately parallel to segments DE, EF and FA, respectively. The effective stiffness corresponding to these three cases are calculated according to equation (7) and plotted in Fig.8, showing a clear increasing tendency when the current increases, which matches very well with the stated stiffness variability. Furthermore, Fig.7 also illustrates that when the current I_2=1A, segment CD disappears. The reason is that there is no relative motion between the piston of the upper damper and the upper cylinder while the spring is always working. In order to verify the working principle, the spring deformations under two representative working conditions of I_2 = 0A and I_2=1A are given. The blue curve represents the motion of the pistons. The green curve is the deformation of the spring under I_2 = 0A while the red curve represents its deformation with I_2 = 1A. From this figure, it can be seen that the spring deformation under the condition of I_2 = 0A is much smaller than the spring deformation under I_2 = 1A, which means with the stiffness increases steadily with the increase of I_2.

$$k_{\text{eff}} = \frac{F_{\max} - F_{\min}}{D_{\max} - D_{\min}} \tag{7}$$

where $F_{\max}$ and $F_{\min}$ are the maximum and minimum forces generated by the damper at the maximum and minimum value of the stroke, respectively; $D_{\max}$ and $D_{\min}$ are the maximum and minimum value of the stroke, respectively.

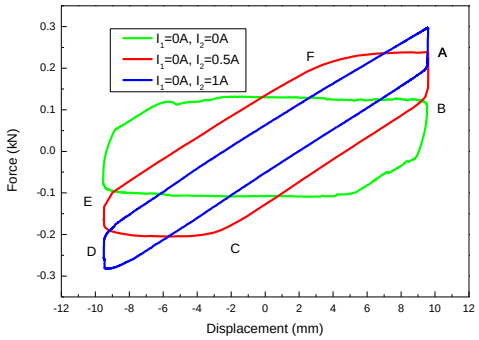

Fig.7. Variable stiffness

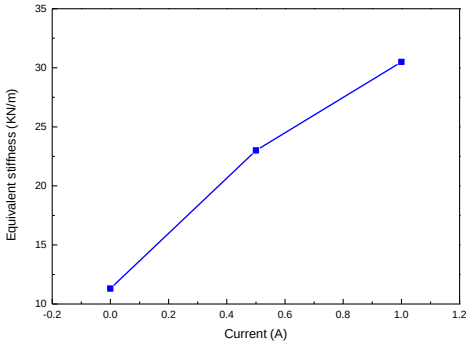

Fig. 8. Equivalent stiffness of MRF damper

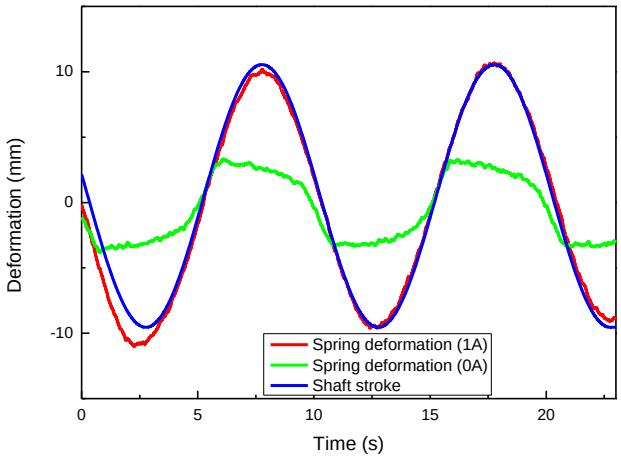

Fig. 9. Spring deformation under different currents.

It should be noticed that the stiffness variation in this test slightly induces damping variation. From Fig, 7, it can be seen that the damping of this damper, indicated by the enclosed area of each loop, decreases when the current I_2 increases. The reason is when the damping of the upper damping cylinder is small (corresponding to low stiffness), relevant displacement between the piston and cylinder exists, which adds damping to this device. However, when the damping of the upper damping cylinder is large enough (corresponding to high stiffness), no relevant displacement exists, which means the damping of this device is smaller.

5.2 Damping Variability

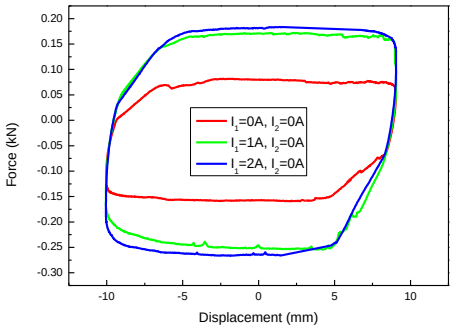

Fig.10. Variable damping

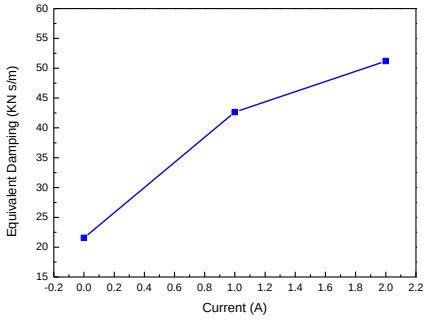

Fig. 11. Equivalent damping of MRF damper

Fig. 10 shows the variable damping characteristic of the damper under different currents of I_1 =0A, 1A, and 2A, respectively. It is seen that the enclosed area of the force-displacement loops increases with the increase of current I_1 and that the peak force shows a saturation trend. This means that increasing I_1 leads to the increase in the equivalent damping of the MRF damper, which can be evidenced by Fig. 11 where the equivalent damping coefficient versus current is shown. It can be seen from Fig. 11 that the increase in current I_1 from 0A to 2A leads to the equivalent damping coefficient being increased from 21.55 KN/(m/s) to 51.21 KN/(m/s). It should be noticed that the dynamic range of the damping is approximately 2 which is lower than conventional MRF dampers due to the saturation of the magnetic field in the shaft of the lower damper piston. The saturation of the magnetic field in the shaft resisted the increase of the magnetic field in the gap area even the current keeps increasing. The dynamic range can be enhanced by enlarging the diameter of the shaft.

5.3 Frequency dependent response

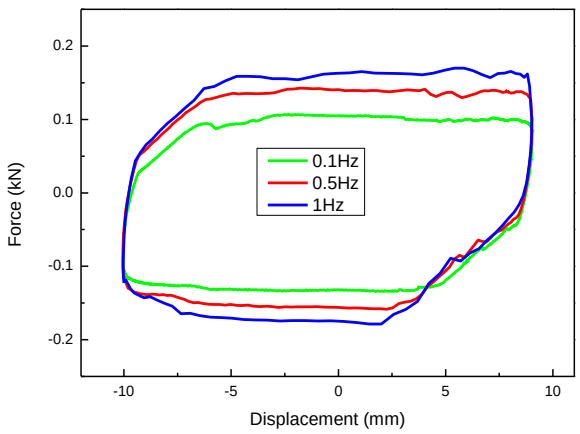

Fig.12. Response to different frequencies

Fig.12 gives an analysis of the effectiveness of changing the loading frequency on the output of the MRF damper. In this test, the loading frequency was chosen as 0.1Hz, 0.5Hz, and 1Hz, with I_1=0A, I_2=0A, respectively. It is seen that, just like the traditional MRF dampers, the peak force and the equivalent damping (area enclosed by the force-displacement loop) increases slightly when the loading frequency increases, and that the effective stiffness is approximately independent of the loading frequency.

5.4 Amplitude-dependent response

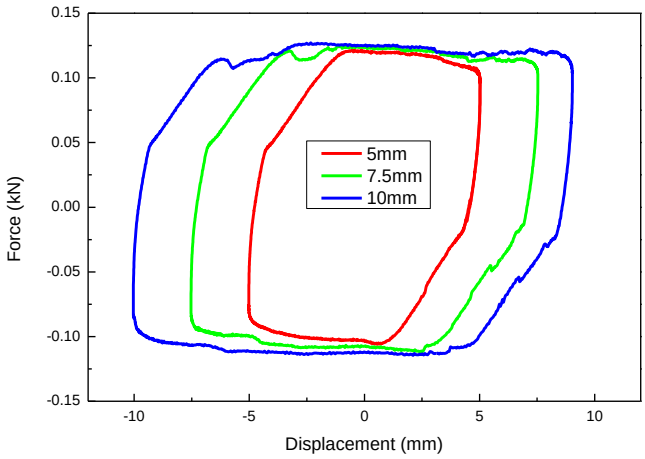

Fig.13. Response to different amplitudes

Fig.13 shows the responses of MRF damper under different loading amplitudes, i.e. 5 mm, 7.5 mm, and 10 mm. The testing frequency is 0.1Hz and the currents are I_1=0A, I_2=0A. It is obvious that the change of amplitude has slight influence on the peak damping force, however, the equivalent damping increases apparently as the amplitude increases. It also can be seen that the effective stiffness tends to be smaller when the amplitude changes to be bigger.

6. MODELLING AND PARAMETER IDENTIFICATION

6.1 Model Establishment

A mathematic model was established to describe the proposed variable stiffness and damping MRF damper. As shown in Fig.14, a coulomb friction element f_1 in parallel with a viscous dashpot c_1 is used to characterize the lower damping cylinder. Similarly, another coulomb friction element f_2 in parallel with a viscous dashpot c_2, in series connection with a spring is

used to describe the upper MRF damper. Among these four parameters, f_1 and c_1 vary their values due to the change of I_1 while f_2 and c_2 is controlled by I_2.

If the current in the upper coil is sufficiently high, the excitation force is smaller than the friction force in element f_2 and the element does not slide, so the viscous dashpot c_2 is blocked. In such case, the spring will be compressed when the external force F has a displacement. The stiffness of the damper is, therefore, represented by the stiffness of spring. Otherwise, a relative motion between the piston rod and the upper damper is possible. The stiffness of the damper in this case can be regarded as approximately 0. To sum up, the stiffness variation is controlled by the regulation of c_2 and f_2. As for the damping variation property, it is mainly dependent on the viscous dashpot c_1 and f_1. The rheological property of viscous dashpot c_1 and f_1 is adjusted by the current applied to the lower damper. In this model, x_2 is the relevant displacement between the top connecter and the bottom connector. x_1 is the relative displacement between the top connecter and the upper MRF damper. The equation for the model can be written as:

$$F_e = c_1\dot{x}_2 + f_1 + k_2x_1 \tag{8}$$

where F_e is the excitation force to the variable stiffness and damping MRF damper. In order to obtain the relationship between F_e and x_2, x_1 is needed to be eliminated. x_1, thererfore, is required to be substituted by $x_2$through the following equations:

$If \;\; f_2 > k_2x_1$

$$x_2 = x_1 \tag{9}$$

$If \;\; f_2 + c_2(\dot{x}_1 - \dot{x}_2) < k_2x_1$

$$f_2 + c_2(\dot{x}_1 - \dot{x}_2) + k_2x_2 = 0 \tag{10}$$

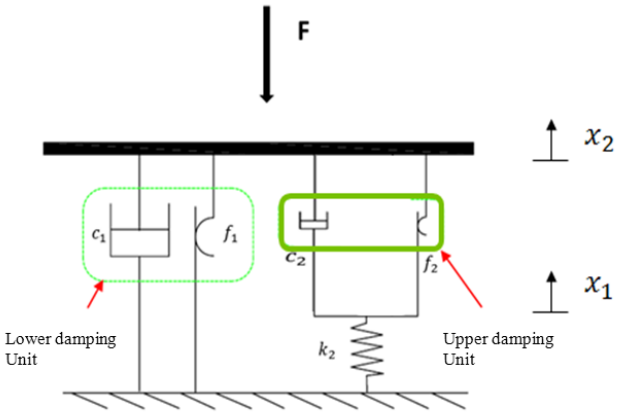

Fig.14. Model of the new MRF damper

6.2 Parameters Identification

To assess the ability to predict the behavior of the proposed damper, the model was fit to the measured data shown in Fig.7 and Fig.10. The first step to determine the proposed model is to identify the corresponding parameters. A total of four parameters, i.e. c_1, c_2, f_1, and f_2, need to be determined by using the least-square method in combination with the Trust-region-reflective algorithm available in MATLAB (R2013b). The main idea of this method is to minimize the value of a function which is chosen as the root mean square between the predicted and the experimentally obtained forces, as indicated by:

$$J = \sum_{i=1}^{N} \sqrt{\frac{(F_{ei} - F_{mi})}{N}} \tag{11}$$

where F_{ei} refers to the i^{th} predicted force, F_{mi} refers to the i^{th} measured force, and N is a neighborhood which is defined as the trust region that can reasonably reflect the behavior of function J. It is clear that the predicted response will approximate the measured response to the greatest degree only if J reaches its minimum value.

As described in section 6.1 that the lower damping unit (c_1 and f_1) mainly presents the property of variable damping and the upper damping unit (c_2 and f_2) presents the property of variable stiffness, therefore, in the identification process, c_1 and f_1 need to be determined while c_2 and f_2 remain constants for the case of variable damping, conversely, c_2 and f_2 have to be identified while c_1 and f_1 remain constants for the case of variable stiffness. Table 2 lists the optimized values for these two cases and Fig.15 and Fig.16 shows the comparison between the predicted and experimentally obtained responses for the stiffness variability and

damping variability, respectively. From an overall point of view, the proposed model predicts the behavior of the damper very well. Fig.15 shows the proposed model has reasonably modeled the property of variable stiffness that the increase of the current increases the effective stiffness of the force-displacement loops, and Fig.16 shows the capability of the model to describe the property of damping variability referring to the increasing enclosed areas of the force-displacement loop induced by the increasing currents.

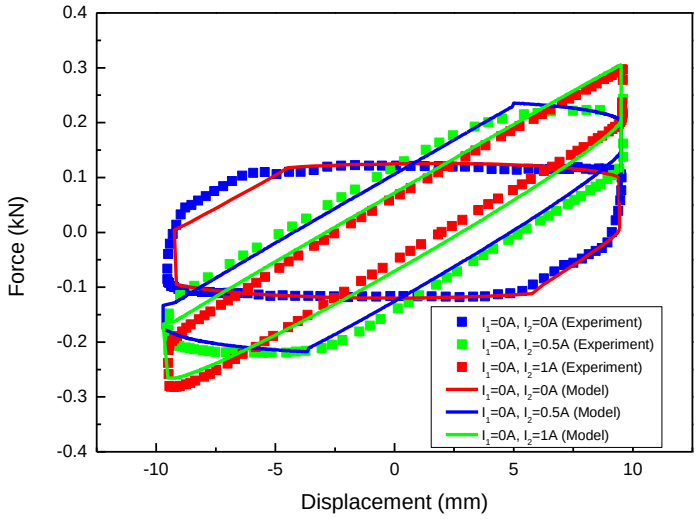

Fig.15. Identification results of variable stiffness

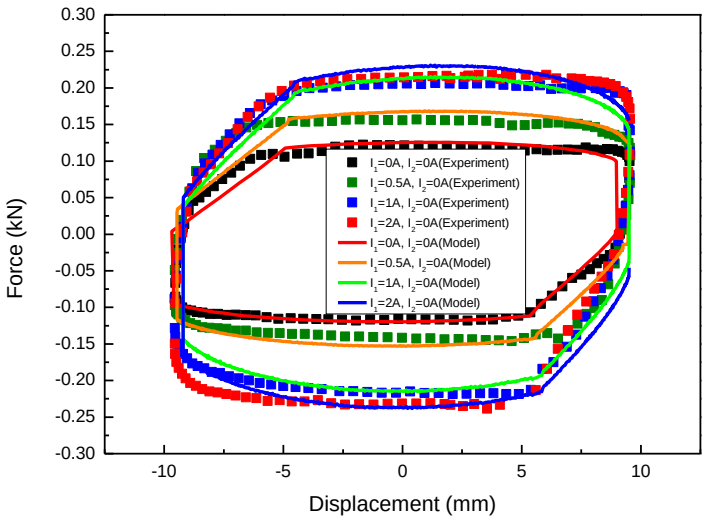

Fig.16. Identification results of variable damping

Table 2. Identification results

Parameters	c_1	f_1	c_2	f_2		Parameters	c_1	f_1	c_2	f_2
I_1=0, I_2=0	54	89	11	89		I_1=0, I_2=0	54	89	11	89
I_1=0.5, I_2=0	72	169	11	89		I_1=0,I_2=0.5	54	89	17	323
I_1=1, I_2=0	153	237	11	89		I_1=0, I_2=1	54	89	23	512
I_1=2, I_2=0	159	271	11	89						

In order to fully verify the capability of the proposed model to predict the performance of the damper and evaluate the validity of the identified parameters shown in Table 2, different data sets were used to see the effectiveness of the model by using those identified values for the parameters. As shown in Fig.17 (a), the model with those parameters was fitted to difference responses under different amplitudes. It can be seen from Fig.17 (a) that excellent agreement was found between the predicted and measured responses, which means the parameters listed in Table 2 can also precisely describe the new testing results. As shown in Fig.17 (b), the testing results with I_1=0.5A and I_2 =0A, 0.5A, 1A were further used to verify the model performance. As parameters c_1 and f_1 are independent of c_2 and f_2, the parameters c_1 and f_1 were chosen as 72 and 169 according to the identification results of I_1=0.5, I_2=0 while the parameters c_2 and f_2 were chosen from the identification results of I_1=0, I_2=0A, 0.5A, 1A. From the fitting results in Fig.17 (b), it can be seen that the identification results in table 2 are also suitable for the new testing results. To conclude from the above analysis and comparison, the proposed model is appropriate for the description of the dynamic performance of the damper.

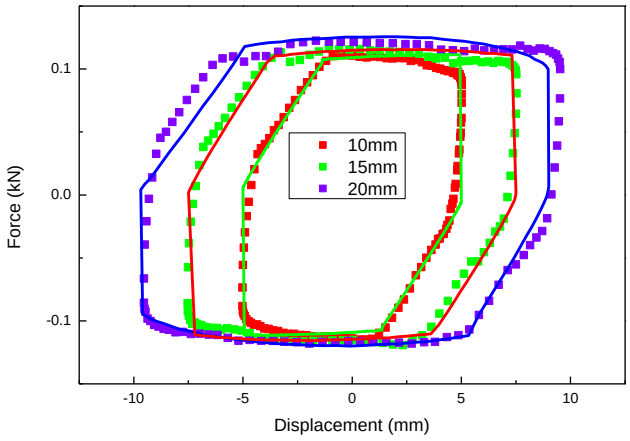

(a)

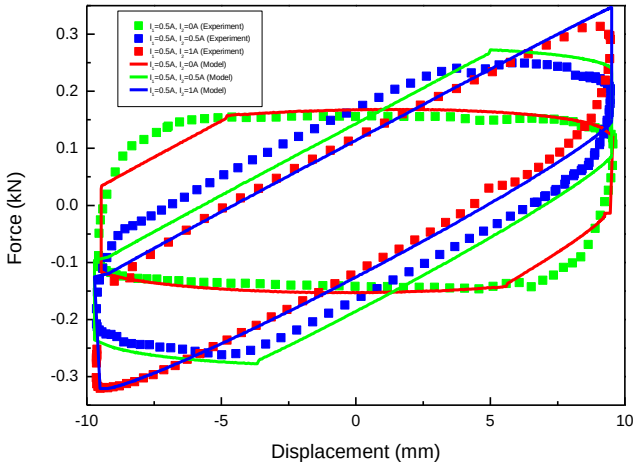

(b)

Fig.17. Fitting results of model verification

7. Conclusion

This study designed, developed, tested, and modelled a compact variable stiffness and damping MRF damper. The analysis and test results verified that both the stiffness and the damping properties of the damper can be controlled. The stiffness of the damper can vary from 11.3kN/m to 30.5kN/m when the current applied to the upper damping cylinder is increased from 0A to 1A. The equivalent damping coefficient has the ability to change from 21.55 KN/(m/s) to 51.21 KN/(m/s). It should be noticed that the stiffness cannot be changed totally independent of the damping due to the fact that the spring stiffness is constant and not variable. An innovative model was established and identified to describe the proposed MRF damper. The successful development of the variable stiffness and damping proves the concept of variable stiffness and damping feasible.

Acknowledgements

This research is supported by ARC Discovery Grants (Nos. 150102636, 140100303), the National Natural Science Foundation of China (Nos. 51205100, & 51328502), and the University of Wollongong and China Scholarship Council joint scholarships.

References:

[1] S.B. Choi and Y.M. Han, “Vibration control of electrorheological seat suspension with human-body model using sliding mode control,” Journal of Sound and Vibration, vol. 303, no. 1, pp. 391-404, Jun.2007.

[2] S. Sun, H. Deng, and W. Li., "A variable stiffness and damping suspension system for trains," Proc. SPIE 9057, Active and Passive Smart Structures and Integrated Systems, conference Volume 9057, Mar. 2014.

[3] J. Yang, S. S. Sun, H. Du, W. H. Li, G. Alici, H. X. Deng, "A novel magnetorheological elastomer isolator with negative changing stiffness for vibration reduction, " Smart Materials and Structures, vol. 23, no. 10, 105023, Oct. 2014.

[4] S. Sun, Y. Chen, J. Yang, T. Tian, H. Deng, W. Li, H. Du, and G. Alici,"The development of an adaptive tuned magnetorheological elastomer absorber working in squeeze mode," Smart Materials and Structures, vol. 23, no. 7, 075009, July 2014.

[5] H. Du, K. Yim Sze, J. Lam, "Semi-active H∞ control of vehicle suspension with magneto-rheological dampers," Journal of sound and vibration, vol. 283, pp. 981-996, 2005.

[6] S. B. Choi and W. K. Kim, "Vibration control of a semi-active suspension featuring electrorheological fluid dampers," Journal of sound and vibration, vol. 234, pp. 537-546, 2000.

[7] Y. T. Choi and N. M. Wereley, "Biodynamic response mitigation to shock loads using magnetorheological helicopter crew seat suspensions," Journal of aircraft, vol. 42, pp. 1288-1295, 2005.

[8] W. Li, H. Du, N. Guo, "Design and testing of an MR steering damper for motorcycles," The International Journal of Advanced Manufacturing Technology, vol. 22, pp. 288-294, 2003.

[9] S. Sun, H. Deng, W. Li, H. Du, Y. Q. Ni, J. Zhang, and J. Yang, “Improving the critical speeds of high-speed trains using magnetorheological technology,” Smart Materials and Structures, vol. 22, no. 11, 115012, Nov. 2013.

[10] M. Yu, C. Liao, W. Chen, and S. Huang, “Study on MR semi-active suspension system and its road testing,” Journal of Intelligent Material Systems and Structures, vol. 17, no. 8-9, pp. 801-806, Sep. 2006.

[11] G. Yao, F. Yap, G. Chen, W. H. Li, and S. Yeo, “MR damper and its application for semi-active control of vehicle suspension system,” Mechatronics, vol. 12, no. 7, pp. 963-973, Sep. 2002.

[12] M. Yu, X. Dong, S. Choi, and C. Liao, “Human simulated intelligent control of vehicle suspension system with MR dampers,” Journal of Sound and Vibration, vol. 319, no. 3, pp. 753-767, Jan. 2009.

[13] R. Li, W. Chen, M. Yu, and D. Liu, “Fuzzy intelligent control of automotive vibration via magneto-rheological damper,” in IEEE Conference on Cybernetics and Intelligent Systems (CIS), Dec. 2004, pp. 503-507.

[14] I. Youn and A. Hać, “Semi-active suspensions with adaptive capability,” Journal of Sound and Vibration, vol. 180, no. 3, pp. 475-492, Feb. 1995.

[15] Y. Li, J. Li, T. T, and W. Li, "A highly adjustable magnetorheological elastomer base isolator for applications of real-time adaptive control," Smart Materials and Structures, vol. 22, no. 9, pp. 095020, Sep. 2013.

[16] M. Behrooz, X.Wang, and F. Gordaninejad , "Modeling of a new semi-active/passive magnetorheological elastomer isolator," Smart Materials and Structures, vol. 23, no. 4, pp. 045013, April 2014.

[17] P. Raja, J. Wang, and F. Gordaninejad., "A high-force controllable MR fluid damper–liquid spring suspension system," Smart Materials and Structures, vol. 23, 015021, Jan. 2014.

[18] Y. Liu, H. Matsuhisa, H. Utsuno, and J. G. Park, "Vibration isolation by a variable stiffness and damping system," JSME International Journal Series C, vol. 48, no. 2, pp. 305-310, Dec. 2005.

[19] Y. Liu, H. Matsuhisa, and H. Utsuno, "Semi-active vibration isolation system with variable stiffness and damping control," Journal of Sound and Vibration, vol. 313, no. 1, pp. 16-28, Jun. 2008.

[20] C. Spelta, F. Previdi, S. M. Savaresi, P. Bolzern, M. Cutini, C. Bisaglia, and S. A. Bertinotti, "Performance analysis of semi-active suspensions with control of variable damping and stiffness," Vehicle System Dynamics, vol. 49, no. 1-2, pp. 237-256, Jul. 2011.

[21] Y. Xu and M. Ahmadian, "Improving the capacity of tire normal force via variable stiffness and damping suspension system," Journal of Terramechanics, vol. 50, no. 2, pp. 121-132, Apr. 2013.

[22] Y. Xu, M. Ahmadian, and R. Sun, "Improving Vehicle Lateral Stability based on Variable Stiffness and Damping Suspension System via MR Damper," IEEE Transactions on Vehicular Technology, vol. 63, no. 3, pp. 1071-1078,Sep. 2014.

[23] C. Greiner-Petter, A. Tan, and T Sattel, "A semi-active magnetorheological fluid mechanism with variable stiffness and damping," Smart materials and structures, vol. 23, 115008, Oct. 2014.

[24] W. Li, X. Y. Wang, X. Z. Zhang, Y. Zhou, "Development and analysis of a variable stiffness damper using an MR bladder," Smart materials and structures, vol. 18, no.7, 074007, 2009.

[25] X. Zhang, X. Wang, W. Li, and K. Kostidis, "Variable stiffness and damping MR isolator," in Journal of Physics: Conference Series, vol. 149, no.1, 012088, 2009.